



Photocatalytic reduction of CO₂ to methanol by three-dimensional hollow structures of Bi₂WO₆ quantum dots



Zaiyong Jiang^{a,b}, Xizhuang Liang^a, Hailong Zheng^a, Yuanyuan Liu^{a,*}, Zeyan Wang^a, Peng Wang^a, Xiaoyang Zhang^a, Xiaoyan Qin^a, Ying Dai^a, Myung-Hwan Whangbo^c, Baibiao Huang^{a,*}

^a State key Laboratory of Crystal Materials, Shandong University, Jinan 250100, PR China

^b Key Lab of Pulp and Paper Science and Technology of Education Ministry of China, Qilu University of Technology, Jinan 250353, PR China

^c Department of Chemistry, North Carolina State University, Raleigh, NC 27695-8204, USA

ARTICLE INFO

Article history:

Received 23 March 2017

Received in revised form 6 July 2017

Accepted 10 July 2017

Available online 11 July 2017

Keywords:

Bi₂WO₆

Hollow structure

Photocatalysts

CO₂ photoconversion

Quantum size effect

ABSTRACT

Three-dimensional hollow structures made up of Bi₂WO₆ quantum dots were prepared by one-pot solvothermal synthesis using ethylene glycol as reactive solvent. The structural, optical and CO₂-photoreduction to methanol of these hollow structures were investigated. The ethylene glycol is important not only in assembling the three-dimensional hollow structures but also in suppressing the agglomeration of Bi₂WO₆ quantum dots. The hollow structure of Bi₂WO₆ quantum dots has a much higher CO₂ adsorption capacity and a wider band gap than does bulk-Bi₂WO₆, so that the CO₂ photoconversion reaction is much faster for the hollow structures made up of Bi₂WO₆ quantum dots.

© 2017 Published by Elsevier B.V.

1. Introduction

The photocatalytic reduction of CO₂ into valuable fuels with H₂O was first demonstrated in 1978 [1]. Since then artificial photosynthesis has attracted much attention owing to its potential in solving the environmental problems of the greenhouse gas, CO₂ [2–8]. Semiconductor photocatalysts such as CdS [9], GaP [10], as well as organic compounds [11,12] have been examined for CO₂ conversion under solar irradiation. However, most suffer from serious photocorrosion, making the process of artificial photosynthesis unstable. Oxide-based semiconductors are known to be suitable for CO₂ photoreduction due to their chemical stability. Bismuth tungstate Bi₂WO₆ is a photocatalyst with band gap of ~2.8 eV, and is nontoxic, highly photostable, thermally stable and eco-friendly. Thus, it is important for solar energy conversion and organic pollution purification, in particular, CO₂ photoconversion from an aqueous environment [13–15]. Bi₂WO₆ is made up of (Bi₂O₂)²⁺ and (WO₄)²⁻ layers, which share their oxygen corners and alternate along the c-direction (Fig. S1) [16]. This unique layered structure facilitates the separation of photogenerated electrons and holes and

hence enhances the photocatalytic activity [17]. However, Bi₂WO₆ is poor in photoreducing CO₂ because its CO₂ uptake is low and its surface active sites are limited in number [15]. An important challenge in enhancing the CO₂ photoreducing activity of Bi₂WO₆ is to increase the CO₂ uptake and expose more active surface sites.

So far, many attempts have been made to meet this challenge. Atomically-thin Bi₂WO₆ samples [15] are efficient for solar CO₂ conversion because they possess abundant catalytically-active sites and their quantum size effect, which increases the band gap hence raising the conduction band minimum (CBM) and enhancing the rate of CO₂ photoconversion. Bi₂WO₆ hollow microspheres [13] are efficient for CO₂ conversion because they increase the capacity for CO₂ uptake. To take the advantages of these two observations, one might consider assembling atomically-thin Bi₂WO₆ layers or Bi₂WO₆ quantum dots (QDs) to form a three-dimensional (3D) hollow structure made up of Bi₂WO₆ QDs. In general, it is difficult to prepare atomically-thin Bi₂WO₆ layer or Bi₂WO₆ QDs without getting them aggregated. A substantial quantum size effect occurs in ultrathin two dimensional layer and zero-dimensional QDs. For practical applications as well as scientific curiosity, it is important and interesting to explore a method with which to construct a 3D hollow structure made up of Bi₂WO₆ QDs.

In this paper, we successfully assemble Bi₂WO₆-QDs into a 3D Bi₂WO₆ hollow structure by using a one-pot solvothermal method,

* Corresponding authors.

E-mail addresses: yyliu@sdu.edu.cn (Y. Liu), bbhuang@sdu.edu.cn (B. Huang).

which exhibits a large specific surface area. The band gaps of QD6-Bi₂WO₆, QDh-Bi₂WO₆ and bulk Bi₂WO₆ are evaluated to be 3.10 eV, 2.98 eV and 2.69 eV, respectively. The valence band XPS spectra shows their VB positions are at about 1.95 eV, 2.26 eV and 2.08 eV. The respective CB positions can be calculated to be –1.15 eV, –0.72 eV and –0.61 eV. As far as we know, this is firstly reported that three-dimensional structure can display quantum size effect, leading to the broadening of band gap. Moreover, the QDh-Bi₂WO₆ exhibits much higher CO₂ adsorption capacity than that of bulk Bi₂WO₆, which is in favour of CO₂ photoconversion activity. The quantum size effect and improved CO₂ adsorption capacity give the good explanations for the enhanced CO₂ photoconversion property of QDh-Bi₂WO₆.

2. Experimental

2.1. Materials

Bi(NO₃)₃·5H₂O, Na₂WO₄·2H₂O, and ethylene glycol were provided from the Sinopharm Chemical Reagent Corporation (Shanghai, China). All materials, which were analytical grade, were used without further purification in this study.

2.2. Synthesis of photocatalysts

QDh-Bi₂WO₆ was prepared via one-pot simple solvothermal method. Firstly, Bi(NO₃)₃·5H₂O (1.2 mmol, 2.4 mmol, 4.8 mmol, 7.2 mmol, 9.6 mmol, 12 mmol), and Na₂WO₄·2H₂O (0.6 mmol, 1.2 mmol, 2.4 mmol, 3.6 mmol, 4.8 mmol, 6 mmol,) were dissolved into 40 mL ethylene glycol, respectively. These two solutions were mixed together with vigorous stirring for 1 h. Afterwards the mixture was transferred into a 100 mL Teflon-lined stainless autoclave, which was maintained at 160 °C for 15 h. The corresponding products were marked as QD1-Bi₂WO₆, QD2-Bi₂WO₆, QD3-Bi₂WO₆, QD4-Bi₂WO₆, QD5-Bi₂WO₆, QD6-Bi₂WO₆. The QD2-Bi/EO [Bi(NO₃)₃·5H₂O (2.4 mmol)] and QD6-Bi/EO [Bi(NO₃)₃·5H₂O (12 mmol)] were prepared according to above condition except without the addition of Na₂WO₄·2H₂O and the reaction time for 8 h. Moreover, QD6-Bi₂WO₆ was heated at 300 °C with the heating rate of 5 °C per minute for 3 h, which is denoted as QDh-Bi₂WO₆. Meanwhile, the bulk Bi₂WO₆ was obtained according to the literature

[18]. Bi₂O₃ and WO₃ were uniformly mixed with 1:1 molar ratio using an ethanol solution and dried at 80 °C for 5 h. The as-prepared powder was sintered at 900 °C for 12 h in air.

2.3. Characterization

The X-ray powder diffraction (XRD) measurements of the as-prepared samples were carried out on a Bruker AXS D8 advance powder diffractometer with Cu K α X-ray radiation. The size and morphology of the sample were measured on a Hitachi S-4800 microscope with an accelerating voltage of 7.0 kV. Transmission electron microscope (TEM) and high-resolution transmission electron microscopy (HRTEM) measurements were examined via a JEOL-2100 microscope. The UV-vis diffuse reflectance spectrum was measured on a Shimadzu UV 2550 recording spectrophotometer equipped with an integrating sphere with BaSO₄ as a reference. A Micromeritics ASAP 2020 analyzer was used to measure the Brunauer-Emmett-Teller (BET) surface areas of the samples at liquid nitrogen temperature. The infrared (IR) spectra were performed on a Fourier transform infrared spectrometer. Time-resolved PL spectra were performed at the emission of 450 nm under 377 nm excitation. The XPS was characterized via using a Thermo Fisher Scientific (ESCALAB 250) X-ray photoelectron spectrometer and the result was charge corrected to the adventitious C 1s peak at 284.8 eV.

2.4. Photocatalytic CO₂ reduction evaluation

The process of photocatalytic reduction of CO₂ is follows: 0.2 g sample was mixed into 100 mL water with vigorous stirring, and high purity CO₂ gas was continuously bubbled through the solution for 1 h before the lamp turn on. A 300 W Xe arc lamp (PLS-SXE300, Beijing Trusttech Co., Ltd.) was used as the light source. The temperature of reactor of photocatalytic CO₂ reduction was controlled at 0° to increase the solubility of CO₂ via using cooling water circulation. At the given time interval, the aqueous solution was withdrawn and the product was monitored by Varian CP-3800 gas chromatograph (FID detector, Propark Q column).

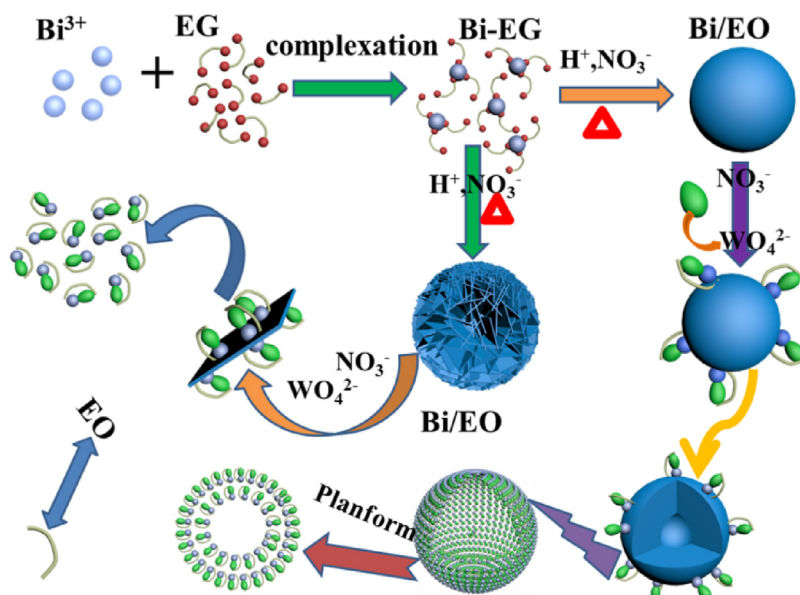


Fig. 1. Schematic representation of the growth process of QDn samples.

3. Results and discussion

As depicted in Fig. 1, EG used as a reactive solvent plays important roles in the preparation of Bi_2WO_6 QDs and the formation of hollow structure of these QDs. The Bi^{3+} ions form Bi-EG complexes with EG, as confirmed by the FT-IR spectra of EG before and after the addition of Bi^{3+} ions. Fig. 2a shows that the O–H vibrational peak frequency (3343 cm^{-1}) of EG is lowered in the presence of Bi^{3+}

ions, which is attributed to the complexing effect. Subsequently, the Bi-EG complexes are transformed into Bi/EO complexes, where EO represents the oxidation product of EG, which is confirmed by their FT-IR spectra (Fig. S2). The Bi/EO complexes display a spherical structure when a high concentration of $\text{Bi}(\text{NO}_3)_3 \cdot 5\text{H}_2\text{O}$ is used for the synthesis, but a flower-like nano structure when a low concentration is used (Fig. S3). The Bi/EO complexes gradually decompose

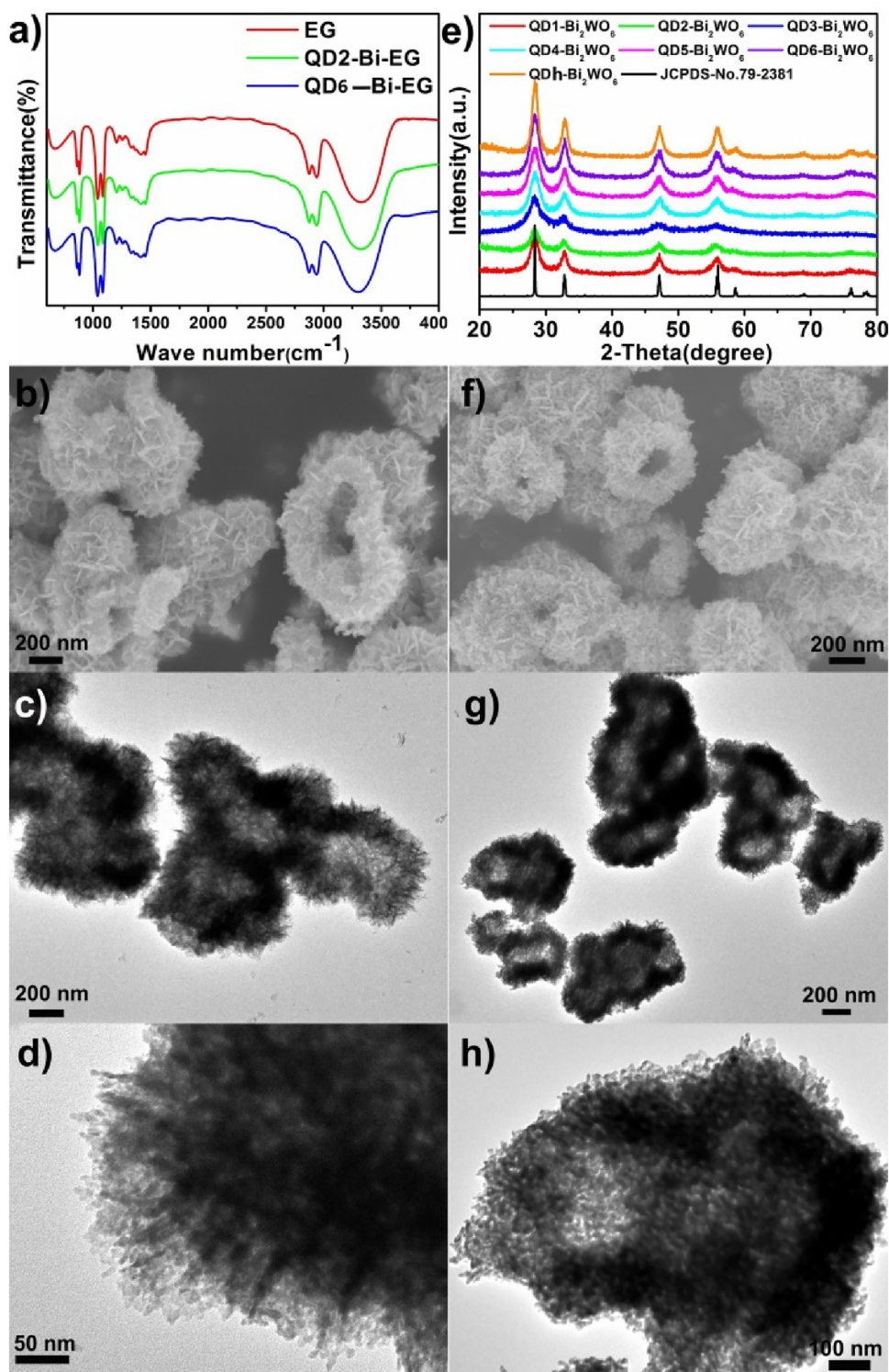


Fig. 2. a) FT-IR spectra of EG, QD2-Bi-EG and QD6-Bi-EG. b) SEM image of QD6. c,d) TEM images of QD6. e) XRD patterns of QDh and QDn. f) SEM image of QDh. g,h) TEM images of QDh.

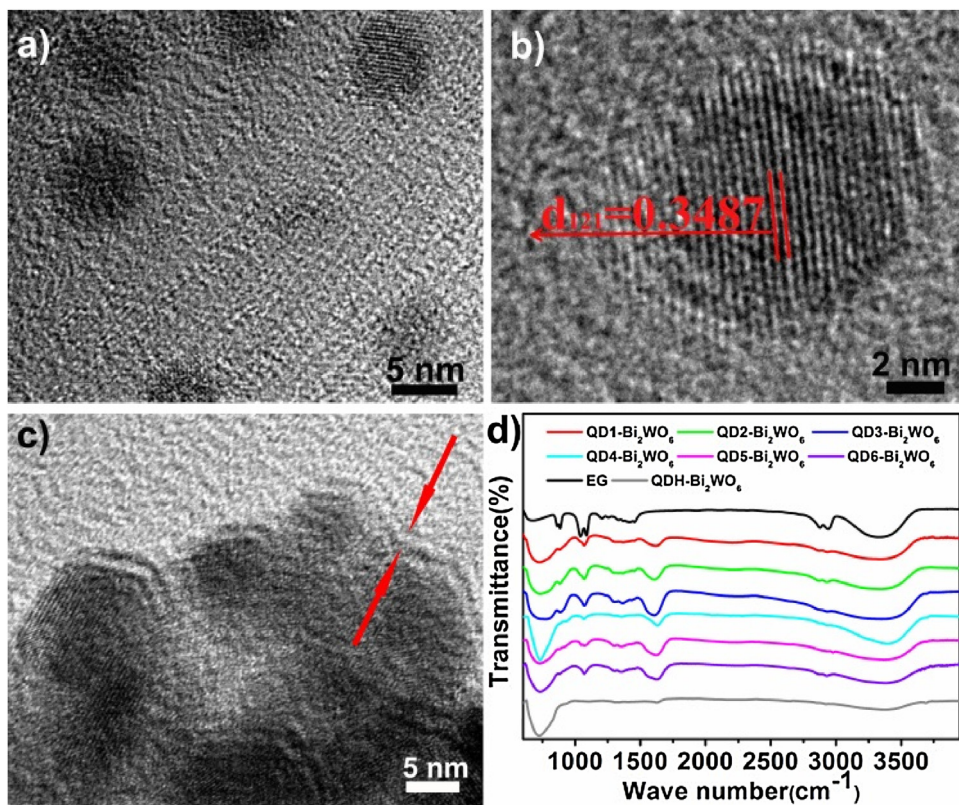


Fig. 3. a–c) HRTEM images of QD6. d) FT-IR spectra of QDn and QDh.

to release the Bi³⁺ ions, which react with (WO₄)²⁻ groups to form Bi₂WO₆ crystals.

QDn ($n=1\text{--}4$) samples have a morphology of disordered nanoparticles (Fig. S4), but QDn ($n=5, 6$) samples a hollow structure (Figs. S4, 2b, 2c). When the (WO₄)²⁻ ions react with the Bi/EO complexes, the Bi³⁺ ions are gradually released to the surface of the spherical structure or the unit flake of the flower-like nano structure to form Bi₂WO₆ crystals. As a consequence, the spherical structure slowly gives rise to a hollow interior, and the sheet structure gradually collapses to form some disordered Bi₂WO₆ nanoparticles. Fig. 2d suggests that the hollow structure consists of very small nanoparticles. The EDS spectra (Fig. S5) show that the W/Bi ratio is about 1:2, corresponding to the theoretical value for Bi₂WO₆.

As-prepared samples were examined by X-ray powder diffraction (XRD) (Fig. 2e, S1b). The diffraction peaks for all samples can be perfectly identified as the orthorhombic Bi₂WO₆ phase (JCPDS, No. 79-2381). The HRTEM images of QD6 (Fig. 3a–c) show that the average particle size of these small nanoparticles is about 6 nm (Fig. 3a), and the measured lattice spacing is about 0.3487 nm (Fig. 3b), which is close to the d-spacing of the 121 planes of Bi₂WO₆ (0.3488 nm). The QDn samples are covered with a thin layer (Fig. 3c). To probe the nature of this layer, we compare the FT-IR spectra of QDn, QDh and EG (Fig. 3d). The latter indicate the presence of EO in QD6, and hence the EO should be the thin layer. This layer suppresses the agglomeration Bi₂WO₆ crystals, hence allowing small nanoparticles to form. This is also the case for QDn- ($n=1\text{--}5$) samples as can be seen from their FT-IR spectra.

The thin layer of EO covering the surface of QDn samples would have unfavorable effects on the CO₂ photoreduction property, so we heated QD6 at 300 °C for 3 h to eliminate the EO to obtain QDh. The FT-IR spectra of QDh (Fig. 3d) reveal the absence of the characteristic peaks of EO. In addition, the color of QD6 changes to that of normal Bi₂WO₆ upon the heat treatment (see the inset of Fig. 4a).

These two results confirm the elimination of EO. The morphology of QDh is almost the same as that of QD6, aside from a slight agglomeration (Fig. 2f–h), suggesting the morphology is retained after the thermal treatment.

The UV-vis absorption spectra of all samples are presented in Figs. 4a, S6. The absorption edge of QD6 is blueshifted from that of bulk-Bi₂WO₆ (Fig. 4a and b), which is attributed to the quantum size effect. The absorption edge of QDh is slightly redshifted from that of QD6, but is still blueshifted from that of bulk-Bi₂WO₆, showing the presence of quantum size effect in QDh. Using the formula $a\hbar\nu = A(\hbar\nu - E_g)^{n/2}$ [19], the band gaps E_g of QD6, QDh and bulk-Bi₂WO₆ are determined to be 3.10, 2.98 and 2.69 eV, respectively (Fig. 4b).

According to the N₂-adsorption isotherm measurements (Fig. S7), QD6 has a large specific surface area (90.7 m²/g) and a small average pore size (4.7 nm). The corresponding values for QDh are greater (42.9 m²/g and 10.3 nm, respectively), which indicates that the elimination of EO results in a slight agglomeration of Bi₂WO₆ QDs. Nevertheless, the specific surface area of both samples is much larger than that of bulk-Bi₂WO₆ (i.e., 0.7 m²/g [15]). From the valence band XPS spectra of QD6, QDh and bulk-Bi₂WO₆ (Fig. 4c), their valence band maximum (VBM) positions are determined to be 1.95, 2.26 and 2.08 eV, respectively. These values together with the band gaps determined already, the CBM positions of QD6, QDh and bulk-Bi₂WO₆ are calculated to be -1.15, -0.72 and -0.61 eV, respectively. The CBM of QDh is slightly higher than that of bulk-Bi₂WO₆, so QDh will have a greater reducing power and hence a higher reaction rate for CO₂ photoconversion. In addition, the VBM is slightly lower for QDh than for bulk-Bi₂WO₆, so the O₂ evolution rate from water would be greater for QDh. The latter indirectly improves the rate for CO₂ photoreduction for QDh. The high resolution XPS spectra of the Bi 4f, O 1s and W 4f binding energy regions are shown in Fig. S8.

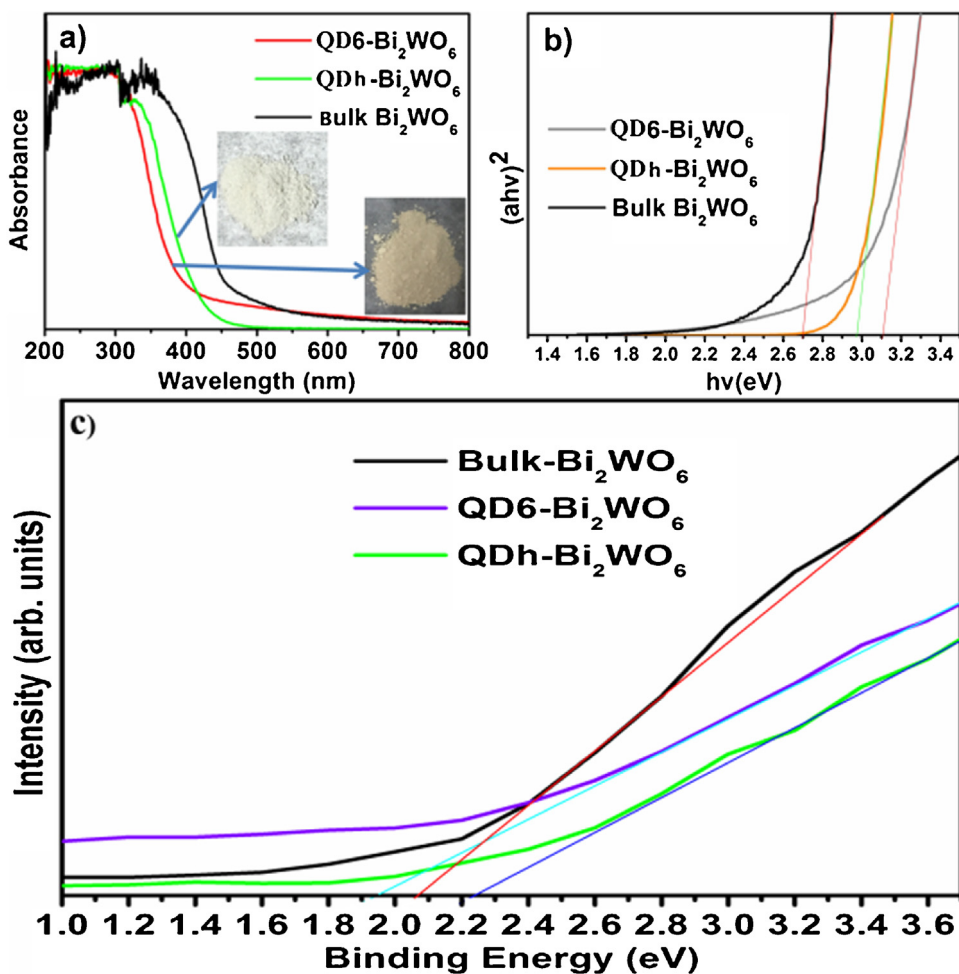


Fig. 4. a) UV–vis absorption spectra and b) band gaps images of QDh, QD6 and bulk-Bi₂WO₆. c) Valence band XPS spectra of QDh, QD6 and bulk-Bi₂WO₆.

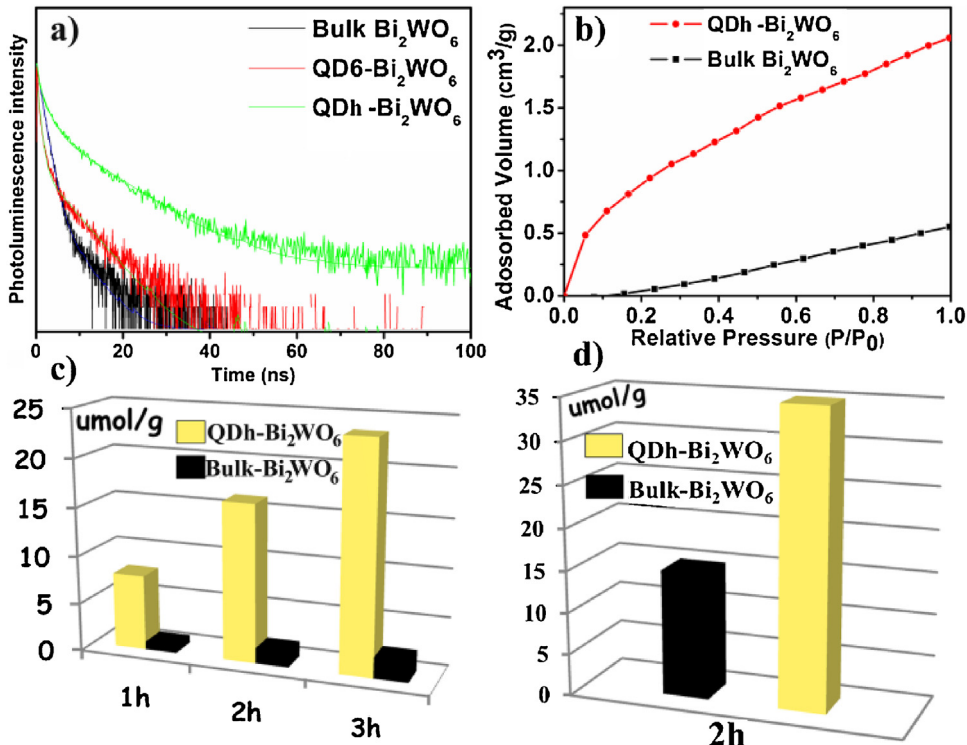


Fig. 5. a) Time-resolved PL spectra for QDh, QD6 and bulk-Bi₂WO₆. b) CO₂ adsorption isotherms on QDh and bulk-Bi₂WO₆ samples at 298 K. c) Photocatalytic CO₂ reduction for QDh and bulk-Bi₂WO₆ samples under UV–vis light irradiation. d) Photocatalytic O₂ evolution of QDh and bulk-Bi₂WO₆.

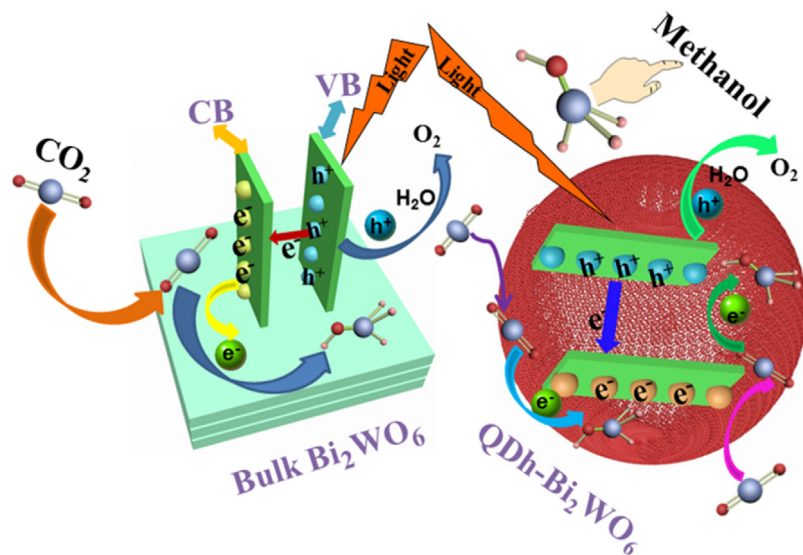


Fig. 6. The Schematic illustration of photocatalytic CO₂ reduction into methanol for QDh-Bi₂WO₆ and bulk Bi₂WO₆.

Time-resolved photoluminescence (PL) spectra of QD6, QDh and bulk-Bi₂WO₆ are presented in Fig. 5a. The average life times of QD6, QDh and bulk-Bi₂WO₆ are evaluated to be 1.85, 6.39 and 1.36 ns, respectively. QDh has the slowest decay rate among the three. A longer lifetime is equivalent to decreasing the recombination rate of photogenerated charge carrier, leading to a more efficient electron-hole separation [20], which is very conducive to photocatalytic activity. Regarding to the different life time between QD6 and QDh, we thought the reason may be due to the thermal treatment. The thermal treatment removes the surface defects and improves the crystallinity of QDh, which is in favour of the migration of photo-generated electron and the hole, thus lead to the enhancement of life time. The CO₂ adsorption isotherms, carried out under ambient conditions (298 K) at low pressure (Fig. 5b), shows that QDh exhibits a much higher CO₂ adsorption capacity compared with that of bulk-Bi₂WO₆. At 298 K and 1 atm, the value for QDh is about four times that of bulk-Bi₂WO₆. Thus, the hollow structure is important in enhancing the CO₂ adsorption capacity. From the PL and absorption isotherm results, it is expected that QDh would be excellent in photocatalytic CO₂ reduction, which we investigated in aqueous solution under UV-vis light irradiation. For comparison, bulk-Bi₂WO₆ was also tested. Here, the main reaction product was identified as methanol by using gas chromatography. Our results shown in Fig. 5c reveal that the CO₂ reduction activity for QDh is about 11 times higher than that of bulk Bi₂WO₆. It is clear that the hollow structure with the quantum size effect is in favour of CO₂ photoreduction and greatly enhances its photocatalytic activity.

A probable mechanism for the photocatalytic CO₂ reaction is depicted in Fig. 6. Under UV-vis light irradiation, QDh (or bulk-Bi₂WO₆) is excited to produce the photogenerated electrons (e⁻) and holes (h⁺). The e⁻ is transferred to the CBM, leaving the h⁺ in the VBM. The latter can oxidize water molecules giving rise to O₂ and protons. The VBM position is lower for QDh than for bulk-Bi₂WO₆ (2.26 vs. 2.08 eV). This would improve the rate for O₂ generation for QDh, indirectly leading to enhance the CO₂ photoreduction rate. This point is confirmed by the photocatalytic O₂ evolution reactions carried out over QDh-Bi₂WO₆ and bulk-Bi₂WO₆ in 100 mL of aqueous solution containing AgNO₃ as a sacrificial reagent. As shown in Fig. 5d, QDh exhibits a much higher O₂ evolution activity than does bulk-Bi₂WO₆. On the other hand, the e⁻ on the CBM can reduce adsorbed CO₂ molecules to methanol under the assistance of the protons. The CBM position is higher for QDh than for bulk-Bi₂WO₆ (-0.72 vs. -0.61 eV), so the CO₂ photoreduction would be greater

for QDh. The origin of this enhancement of the CO₂ photoconversion rate is the result of the quantum size effect. Furthermore, the 3D hollow structure enhances the CO₂ adsorption capacity. The two factors are the reasons why the CO₂ photoreduction efficiency of QDh is better than that of bulk-Bi₂WO₆.

4. Conclusions

In summary, by using one-pot simple solvothermal method, we assembled Bi₂WO₆ QDs with quantum size effect into a 3D hollow structure of Bi₂WO₆ QDs, which has a large specific surface area. QDh-Bi₂WO₆ exhibits much higher CO₂ adsorption capacity compared to that of bulk Bi₂WO₆, which is in favour of CO₂ photoconversion activity. Time-resolved PL spectra of QDh-Bi₂WO₆ and bulk Bi₂WO₆ have been characterized and the average life times have been evaluated to be 6.39 ns and 1.36 ns. The longer lifetime means more efficient separation of photo-generated electron-hole pairs. In addition, the VBM is lower, but the CBM is higher, for Bi₂WO₆ QDs than for bulk-Bi₂WO₆. Therefore, the CO₂ photoreduction efficiency of QDh-Bi₂WO₆ is better than that of bulk Bi₂WO₆. Constructing a 3D hollow structure made up of Bi₂WO₆ QDs may open a new avenue for the modification of Bi₂WO₆ photocatalyst, which is expected to show more potential applications in CO₂ photoconversion.

Acknowledgments

This work was financially supported by a research Grant from the National Basic Research Program of China (the 973 Program, No. 2013CB632401), the National Natural Science Foundation of China (Nos. 21333006, 21573135, 11374190, 51002091, 21007031), Taishan Scholar Foundation of Shandong Province, China, Young Scholars Program of Shandong University (2016WLJH16) and the Shandong Province Natural Science Foundation (ZR2014JL008).

Appendix A. . Supplementary material

Supplementary data associated with this article can be found in the online version at <http://dx.doi.org/xx.xxxx/j.apcatb.xx.xx.xx>

Appendix A. Supplementary data

Supplementary data associated with this article can be found, in the online version, at <http://dx.doi.org/10.1016/j.apcatb.2017.07.023>.

References

- [1] M. Halmann, *Nature* 275 (1978) 115–116.
- [2] S.N. Habisreutinger, L.S. Mende, J.K. Stolarczyk, *Angew. Chem. Int. Ed.* 52 (2013) 7372–7408.
- [3] B. Pan, S.J. Luo, W.Y. Su, X.X. Wang, *Appl. Catal. B: Environ.* 168–169 (2015) 458–464.
- [4] S. Xie, Q. Zhang, G. Liu, Y. Wang, *Chem. Commun.* 52 (2016) 35–59.
- [5] G.X. Zhao, H. Pang, G.G. Liu, P. Li, H.M. Liu, H.B. Zhang, L. Shi, J.H. Ye, *Appl. Catal. B: Environ.* 200 (2017) 141–149.
- [6] B. Kumar, M. Llorente, J. Froehlich, T. Dang, A. Sathrum, C.P. Kubiak, *Annu. Rev. Phys. Chem.* 63 (2012) 541–569.
- [7] S.C. Roy, O.K. Varghese, M. Paulose, C.A. Grimes, *ACS Nano* 4 (2010) 1259–1278.
- [8] J. Ding, Y.F. Bu, M. Qu, Y. Yu, Q. Zhong, M.H. Fan, *Appl. Catal. B: Environ.* 202 (2017) 314–325.
- [9] J. Jin, J.G. Yu, D.P. Guo, C. Cui, W.K. Ho, *Small* 11 (2015) 5262–5271.
- [10] E.E. Barton, D.M. Rampulla, A.B. Bocarsly, *J. Am. Chem. Soc.* 130 (2008) 6342–6344.
- [11] S. Sato, T. Morikawa, T. Kajino, O. Ishitani, *Angew. Chem. Int. Ed.* 52 (2013) 988–992.
- [12] M.D. Doherty, D.C. Grills, J.T. Muckerman, D.E. Polyansky, E. Fujita, *Coord. Chem. Rev.* 254 (2010) 2472–2482.
- [13] H.F. Cheng, B.B. Huang, Z.Y. Wang, X.Y. Qin, X.Y. Zhang, Y. Dai, *Chem. Commun.* 48 (2012) 9729–9731.
- [14] T. Jing, Y. Dai, W. Wei, X.M. Ma, B.B. Huang, *Phys. Chem. Chem. Phys.* 16 (2014) 18596–18604.
- [15] L. Liang, F.C. Lei, S. Gao, Y.F. Sun, X.C. Jiao, J. Wu, S. Qamar, Y. Xie, *Angew. Chem. Int. Ed.* 54 (2015) 13971–13974.
- [16] Y. Zhou, Z.P. Tian, Z.Y. Zhao, Q. Liu, J.H. Kou, X.Y. Chen, J. Gao, S.C. Yan, Z.G. Zou, *ACS Appl. Mater. Interfaces* 3 (2011) 3594–3601.
- [17] H.F. Cheng, B.B. Huang, Y. Dai, *Nanoscale* 6 (2014) 2009–2026.
- [18] J.W. Tang, Z.G. Zou, J.H. Ye, *Catal. Lett.* 92 (2004) 53–56.
- [19] L. Chen, S.F. Yin, R. Huang, Q. Zhang, S.L. Luo, C.T. Au, *CrystEngComm* 14 (2012) 4217–4222.
- [20] G.Z. Wang, Q.L. Sun, Y.Y. Liu, B.B. Huang, Y. Dai, X.Y. Zhang, X.Y. Qin, *Chem. Eur. J.* 21 (2015) 2364–2367.